JOURNAL OF GEOPHYSICAL RESEARCH, VOL. 108, NO. A4, 1155, doi:10.1029/2001JA009060, 2003

Effect of the 14 July 2000 solar flare on Earth's FUV emissions

Thomas J. Immel, Stephen B. Mende, Harald U. Frey, and N. Østgaard
Space Sciences Laboratory, University of California, Berkeley, California, USA

G. R. Gladstone
Southwest Research Institute, San Antonio, Texas, USA

Received 5 October 2001; revised 18 September 2002; accepted 4 February 2003; published 15 April 2003.

[1] An X-class solar flare occurring on 14 July 2000 (Bastille Day) marked the initiation of events which led to a powerful geomagnetic storm on 15 July. At the time of the flare the NASA-IMAGE spacecraft was near apogee and observed a global-scale transient increase in far ultraviolet (FUV) emissions of the thermosphere in both the N_2 Lyman-Birge-Hopfield (LBH) band and the O I 135.6-nm line and also in geocoronal emissions of H I at 121.6-nm. Comparison with the solar x-ray flux measured by GOES 10 shows the delayed response of the FUV emissions compared to the peak in x-rays. This lag is attributed to a later peak in EUV emissions, which drive the photoelectron flux in the energy range which is, in turn, most effective in producing N_2 LBH and O I 135.6-nm emissions. Measurements of solar EUV input by Solar and Heliospheric Observatory (SOHO) Charge, Element, and Isotope Analysis System (CELIAS)/Solar Extreme-Ultra-Violet Monitor (SEM) confirm the close correlation between solar EUV and terrestrial FUV emissions. A comparison of the flare-time variation in the signal in each channel of the instrument allows one to (1) determine the variation in resonantly scattered solar emissions and (2) differentiate between emissions created through photodissociation by solar EUV and those driven by terrestrial photoelectron impact. The latter provides a means for positively identifying the dayglow emissions observed in the SI-12 instrument. *INDEX TERMS:* 7519 Solar Physics, Astrophysics, and Astronomy: Flares; 7549 Solar Physics, Astrophysics, and Astronomy: Ultraviolet emissions; 2479 Ionosphere: Solar radiation and cosmic ray effects; *KEYWORDS:* airglow, dayglow, solar flare, photoelectron, FUV, far ultraviolet

Citation: Immel, T. J., S. B. Mende, H. U. Frey, N. Østgaard, and G. R. Gladstone, Effect of the 14 July 2000 solar flare on Earth's FUV emissions, *J. Geophys. Res.*, *108*(A4), 1155, doi:10.1029/2001JA009060, 2003.

1. Introduction

[2] Short-term (1–60 minute) increases in solar photon flux across the solar spectrum are characteristic of solar flares. The irradiance enhancement can be of several orders of magnitude, especially in x-rays [*Walker and Rugge*, 1969; *Parks and Winckler*, 1971]. Increases in prominent UV emission are usually less than a factor of 2 [*Hall*, 1971], while variations in the visible range are quite small. The study by *Donnelly* [1976] provides a detailed review of the temporal variation of different components of the flare phenomenon. The most well known flare effects are those which affect 20th century technology, namely radio and satellite communications, especially applications pertaining to navigation and global positioning [*Horan and Kreplin*, 1980; *Liu et al.*, 1996]. Such technologies depend on the properties of the ionosphere, which can be significantly modified following a powerful solar x-ray flare, which has the initial effect of enhancing lower ionospheric densities. Protons are accelerated to relativistic velocities at solar flares, and can arrive at Earth in numbers sufficient to further enhance lower ionospheric densities within the magnetic polar caps [*Reid and Collins*, 1959].

[3] Satellites can remotely monitor flare-time modifications of the ionosphere by way of the large variation in the abundance of ionospheric photoelectrons which are regularly generated by solar XUV and EUV photons. The photoelectrons in turn excite far ultraviolet (FUV) emissions to a degree determined by the energy spectrum and magnitude of the photoelectron flux combined with the height-density profile of neutral thermospheric constituents [*Richards and Torr*, 1984; *Bailey*, 1995]. Variations in the photoelectron-produced FUV airglow have been observed on timescales of years and months [*Prinz and Meier*, 1971] to scales as short as minutes [*Opal*, 1973]. With new observations from the IMAGE satellite and high time resolution observations of solar XUV and EUV emissions from the Solar and Heliospheric Observatory (SOHO) spacecraft, it is possible to continue this work in the time-scale of the rise and decay of solar flares.

[4] The IMAGE satellite was placed into orbit in March 2000. It is equipped with three FUV imaging instruments,

Copyright 2003 by the American Geophysical Union.
0148-0227/03/2001JA009060$09.00

the Wideband Imaging Camera (WIC), the Spectrographic Imager (SI), and the Geocoronal Photometer (GEO). The first two instruments obtain 2D images of the entire Earth, with angular resolutions of ~0.07° and 0.13°, respectively. WIC is sensitive in the 140.0–190.0-nm range [*Mende et al.*, 2000a], where the primary terrestrial emissions are the Lyman-Birge-Hopfield band emission produced by N_2 and some emissions by N I. Relatively minor emissions of O I at 164.1 nm are also present, though the bright O I lines at 130.4 and 135.6 nm are well suppressed. The SI instrument has a narrow passband, and can simultaneously isolate the 135.6-nm emission of atomic oxygen in the SI-13 channel, as well as Doppler shifted H I Ly-α emissions in the SI-12 channel (~121.8 nm) which are produced by downward traveling H atoms with several keV energy [*Mende et al.*, 2000b]. The SI-12 instrument has a unique sensitivity curve, in that it has a sinusoidal transmission function with peaks every 5 nm, decreasing in amplitude away from 121.8-nm, and reaching 0% transmission at $\lambda < 117.5$ nm and $\lambda > 126.5$ nm. Though the line is near a minimum in transmission, some response of the SI-12 instrument to the 120.0-nm triplet emission of N I is expected, which is of interest for this work (section 3.4). The integration times are approximately 5 seconds for the SI instruments, and 10 seconds for WIC. GEO observations consist of successive 0.33 second counting integrations, resulting in an angular separation between samples of 1°. The field of view of the instrument is also 1°.

[5] The GEO instrument consists of three photometer tubes. The field of view of the central tube lies in the spacecraft body spin plane, while the outer tubes point out of this plane at ±30°. With a passband between 115 and 150 nm, all three are sensitive to the bright terrestrial 121.6-nm (Ly-α) and 130.4-nm emissions of H I and O I, respectively. Only the center tube regularly detects O I emissions, as its field-of-view makes a transit of Earth every two minutes. From spacecraft positions near apogee (8.1 Re), it can be assumed that the outer tubes detect only Ly-α.

[6] The IMAGE satellite was near apogee of its 14-hour orbit on 14 July when at 1005 UT a solar flare commenced with immediate consequences at Earth. These observations are unique in that previously reported flare-time variations of FUV emissions were from low altitude spacecraft, and therefore never measured at a fixed location on Earth. IMAGE is often situated to observe the effects of solar events at fixed positions on Earth for many hours.

[7] The following report is divided into three main sections. Section 2 describes in detail the observations seen in 5 of the FUV instrument channels. A detailed discussion of the meaning of the observations makes up section 3. A summary and conclusion follows in section 4.

2. Flare Effects Observed by IMAGE-FUV, 14 June 2000

2.1. Observations by WIC, SI-13, and SI-12 Imagers

[8] The Bastille Day solar flare is marked by a significant increase in x-ray flux as measured at GOES 10 (reaching the level of X6). In the 1–8 Angstrom range of x-ray emissions, the solar activity resulted in a factor of ~300 increase, with a peak of $6.0 \cdot 10^{-4}$ W m^{-2} at 10:23 UT. GOES proton monitors detected a rapid increase in relativistic solar proton fluxes (>10 MeV) beginning at 10:35 UT, with a peak in proton flux occurring later the following day. At the time of the flare, IMAGE was approaching apogee at approximately 50°N latitude and 1000 Local Time. The brightness of the FUV dayglow can be characterized with the WIC and SI instruments by selecting particular ranges of solar and spacecraft zenith angles (SZA and DZA, respectively) over which the signal levels of the respective instruments are approximately equal, and dwelling on these fixed positions for the duration of the observations. For example, these can be locations at SZA = 56°, DZA = 22° or SZA = 60°, DZA = 35° (in the case of the WIC instrument) where observations result in similar instrumental signal rates. Three images from WIC clearly show the increase in FUV emissions between 1001 and 1030 UT Figure 1, and the subsequent decrease in emissions by 1100 UT. The times at which these images were obtained are indicated with 3 solid vertical lines in the plot of the GOES 10 x-ray flux. The dark marks near the center of the three images indicate the locations of pixels in the range of SZA and DZA which are used to characterize the WIC dayglow variation throughout the flare.

[9] The variations in x-ray and FUV brightnesses are shown together in Figure 2. The average SZA and DZA values are indicated in the upper right corner of each panel. The measured signal of all three FUV imagers increased by a significant amount, with peak values in all imagers occurring 6–8 minutes after the peak in x-rays. A close correspondence of the sudden increases in FUV brightness seen in all 3 channels with the enhancement in x-ray flux is clearly seen, though it is evident in each plot that the time of the peak x-ray flux precedes the peak in FUV emissions. The magnitude of the variation in each channel of the FUV imager is summarized in Table 1. In all these values and above plots, the background signals in each instrument responses have been subtracted. These background levels are determined from off-Earth pixels, and are 400 A-D units, 2.5 counts, and 6.0 counts for the WIC, SI-13, and SI-12 imagers, respectively. Note that WIC signal is reported in Analog-to-Digital (A-D) units, as it does not count photons but an amplified signal resulting from photon impacts on a photocathode. The SI detectors count individual photons.

[10] The counting rates in the imagers are not directly affected by x-rays, though the following solar protons can cause an increase in background counts. This is evident in the slightly heightened WIC signal following the flare. However, these counts only result in a 400–500 count/pixel contamination, while the WIC signal in observations of the sunlit Earth is usually between 3000 and 10,000 counts/pixel. Thus, the S/N ratio is still quite good after the flare. The SI detectors seem particularly resistant to false signals from energetic protons, due probably to the very different detector design [*Mende et al.*, 2000b].

2.2. Observations by GEO Photometers

[11] Effects of the flare on Earth's Ly-α geocoronal emissions are evident in the measurements from the GEO instrument. Figure 3 shows the counting rates from 2 of the three GEO photometers over two spacecraft revolutions, one before the flare (dotted lines) and one during (solid lines). The top plot (Figure 3a) shows responses from GEO tube 1, who's field of view transits Earth every two minutes. The

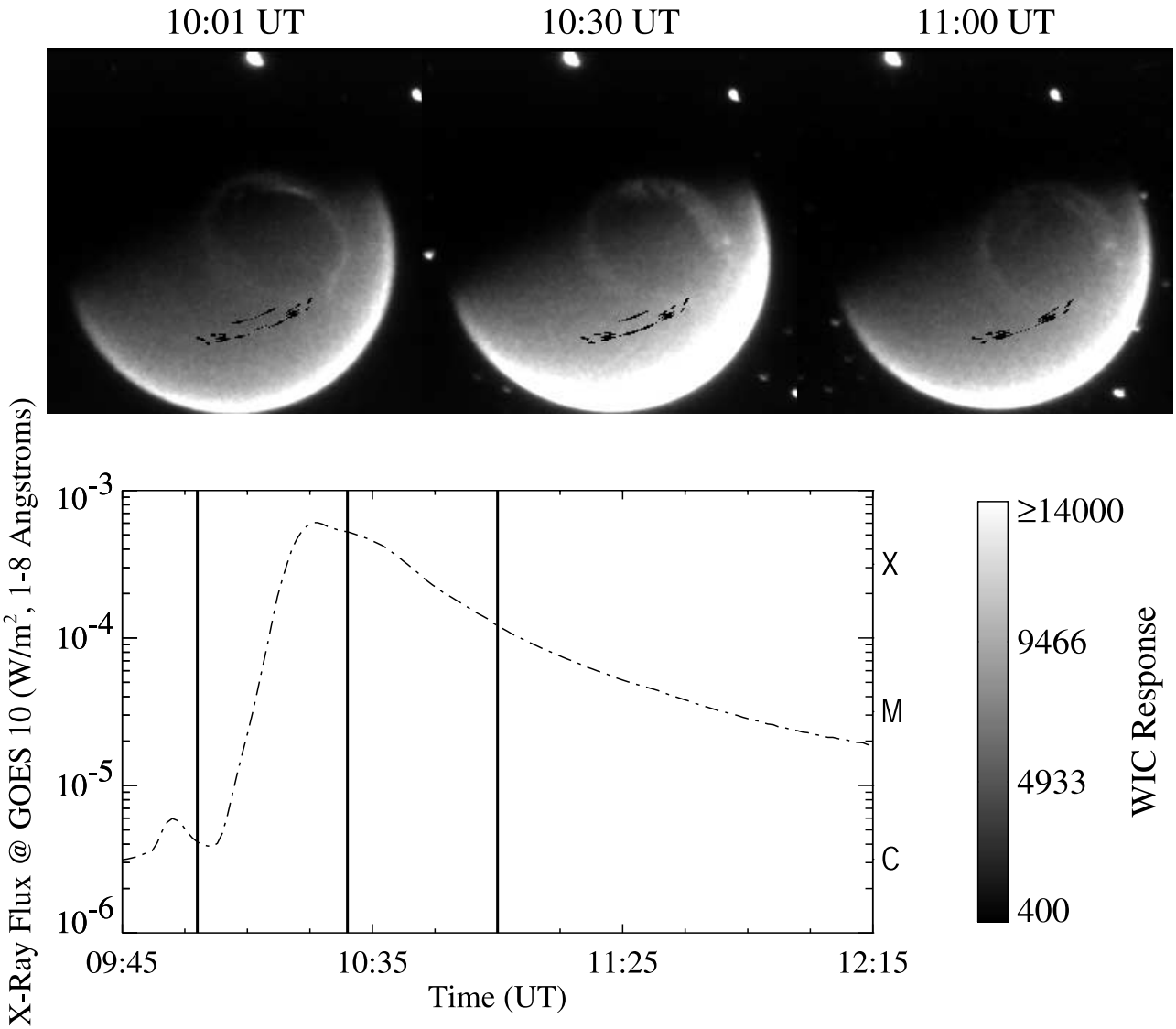

Figure 1. WIC FUV images of Earth during the Bastille Day flare, with GOES 10 x-rays. At top are the images from the FUV WIC channel at preflare, peak flare, and postflare times, shown from left to right, above a summary of the GOES 10 x-ray data. The locations on Earth in particular ranges of SZA and DZA selected to characterize the flare variation are indicated where pixels are blacked out. A careful eye will note the effects of solar energetic protons in the postflare image.

peak counting rate corresponds to an observation of Earth's bright limb, where O I and N I emissions both contribute to the total response. Heightened emissions are also seen on Earth to the right of the peak. Figure 3b shows measurements from GEO tube 2, which from apogee never transists Earth. It therefore measures only geocoronal Ly-α emissions.

[12] The variation of the peak response of each photometer is monitored during the flare. Figure 4 shows the measured peak in the response of GEO tubes 1 and 2 (solid line) during six hours of consecutive 360° scans beginning well before the flare. For comparison, the GEO responses from the same positions along the orbit track during the previous orbit are shown (dotted line). The x-ray flux at GOES is also shown for reference (dot-dashed line).

[13] Regarding the preflare observations of GEO tube 1, whose FOV transits Earth with each spacecraft revolution, one notes that they are consistently between $9 \cdot 10^3$ and $1 \cdot 10^4$ counts. This is because the tangent point at Earth's limb, where the maximum brightness is always observed, has a consistent solar zenith angle (S $\sim$ 50°). The preflare signal in GEO tube 2, whose FOV never transits Earth from altitudes near apogee, shows a more regular variation with altitude, with minimum count rates at apogee, and increases at lower altitudes as the FOV transits regions closer to Earth (greater H density).

[14] With the flare, the response in each GEO tube shows an initial variation similar to those observed in the WIC and SI (Figure 2). After the peak in x-ray flux, the response of GEO tubes 1 and 2 is seen to increase by 20.4% and 10.2%, respectively, then subside to nearly preflare levels over the next 30 minutes. This recovery is interrupted by a second enhancement in photometer response, which in tube 2 grows to more than 30% of previously measured values. The first enhancement corresponds to a flare-time increase

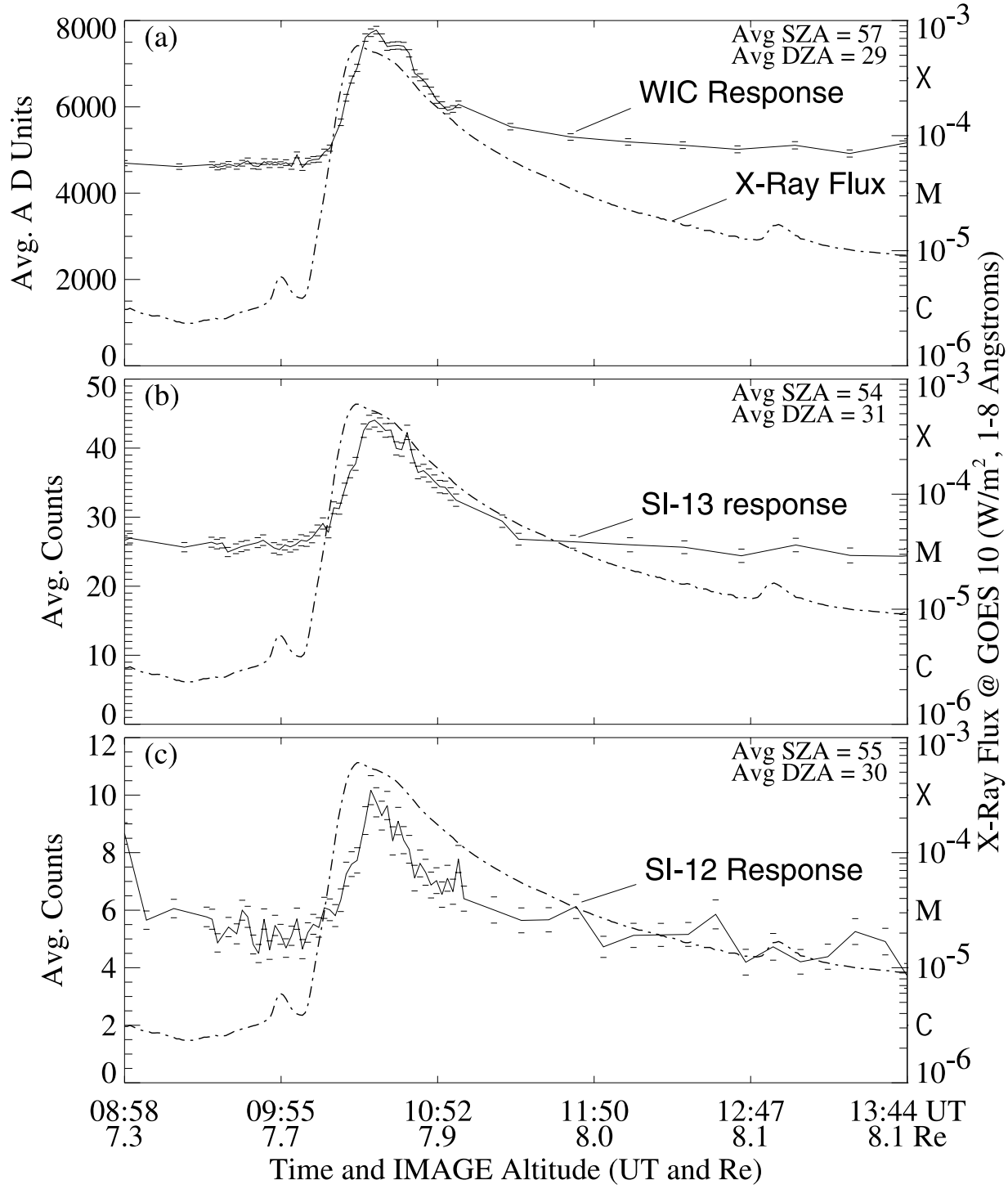

Figure 2. Flare-time variation in the three imaging channels of IMAGE-FUV. 2a) The response in the FUV WIC channel is shown with a solid line, and according to the count rates indicated to the left. The x-ray flux is shown with a dashed line, on a logarithmic scale indicated to the right. The average SZA and DZA of pixels used for the calculation are shown in the upper right of the panel. 2b) Same as 2a except now showing SI-13 response. 2c) Same as 2a except now showing SI-12 response.

in Earth's geocoronal Ly-α emissions, (and in the case of tube one, thermospheric FUV emissions as well) while the second reflects the arrival of high-energy protons from the flare, which subsequently introduce 300–600 extraneous counts per sample in both GEO tubes. Relative to the instrument signals, this additional signal is greater in GEO tube 2 and is therefore more noticeable. The important point is that the proton-produced instrument signal becomes significant only after the peak in the flare-time enhancement of FUV emissions.

[15] The flare-time variation of the GEO tube 1 signal at points on Earth is similar to that seen at the limb (and shown

Table 1. Comparison of FUV Response to Flare in Five IMAGE-FUV Channels

Instrument	PreFMR[a]	Max Response: UT	Percent Change	PostFMR[b]
WIC	4648 A-D units	7700 A-D units - 10:30 UT	65.6 ± 1.1%	5087 A-D units
SI-13	26.0 counts	43.7 counts - 10:30 UT	68.3 ± 2.3%	24.8 counts
SI-12	5.5 counts	9.7 counts - 10:30 UT	76.4 ± 5.1%	4.4 counts
Geo Tube 1	9188 counts	11110 counts - 10:30 UT	20.9 ± 0.6%	9580 counts
Geo Tube 2	3887 counts	4284 counts - 10:32 UT	10.2 ± 0.9%	4903 counts

[a]Preflare mean response.
[b]Postflare mean response.

in Figure 4b). Using the peak in emissions as the reference point indicating the location of the limb, the neighboring sample varies by 21.5%, slightly more than the limb itself. The next point on Earth varies by 17.0%. These values will be used in a later section to further investigate the variation in on-Earth FUV emissions.

3. Discussion

3.1. Comparison of Observed FUV Enhancements

[16] The enhancement in terrestrial FUV brightness is seen in all 3 IMAGE-FUV instruments. Though the variations are nearly simultaneous, the magnitude of the change varies significantly between channels. The preflare and postflare brightness, peak brightness, and percent changes observed with each instrument are summarized in Table 1. There is no significant offset between the times of peak brightness in the instruments. The nearest-neighbor smoothing of the measurements gives a peak brightness at 10:30 UT for all data sets except the off-Earth geocoronal emission (10:32 UT).

[17] The covariation in the off-Earth GEO measurements and the on-Earth Lyman-Birge-Hopfield (LBH), O I and N I measurements is striking. It is well known that the thermospheric airglow emissions such as N_2 LBH are produced by photoelectron impact, a source which is governed by solar EUV fluxes at Earth. Using the geocoronal and thermospheric measurements as proxies for significant solar FUV and EUV emissions, respectively, it can be inferred that the changes in solar fluxes in these two ranges have a similar temporal variation. This indirect observation will be confirmed in a later section. The relative magnitudes of the EUV and FUV fluxes are consistent with variations reported earlier in the literature. The flare-time brightness variations in terrestrial H I and LBH are similar to flare-induced FUV brightenings observed by *Opal* [1973]. In that report, concurrent 10% and 60% variations in OGO-4 zenith measurements of H I 121.6-nm emissions and nadir measurements of N_2 LBH were observed during the 2B-Class flare of 27 December 1968. *Hall and Hinteregger* [1969] also reported a maximum 20% variation in H Ly-α during the most powerful solar flares.

3.2. Determination of Solar O I 130.4-nm Variation

[18] The 10% enhancement at 121.6 nm measured by GEO (tube 2) is matched by a 20% enhancement in combined O I, N I and H I emissions at Earth's limb as measured by GEO tube 1. The major additional contribution to the GEO signal is the O I 130.4-nm emission, with N I 120.0 and O I 135.6-nm emissions adding minor contributions, especially at the limb in the case of the latter emission. The 130.4-nm emission has two components, a terrestrial photoelectron-produced emission (PE), and emissions originating at the Sun and resonantly scattered in the thermosphere (Res). The O I 135.6-nm emission is entirely produced by photoelectron excitation and can be used as a proxy for the flare-time variation in the 130.4-nm PE emission, but the solar 130.4-nm Res source varies by an unknown amount. By combining observations from the SI and GEO instruments, and results from modeling of the GEO instrument's response to terrestrial observations and of the relative brightness of O I(PE) to O I(Res) emissions, the variation in the solar 130.4-nm emission can be extracted.

[19] Combined emissions of H I, O I, and N I observed by GEO are simulated by combining modeled geocoronal H I

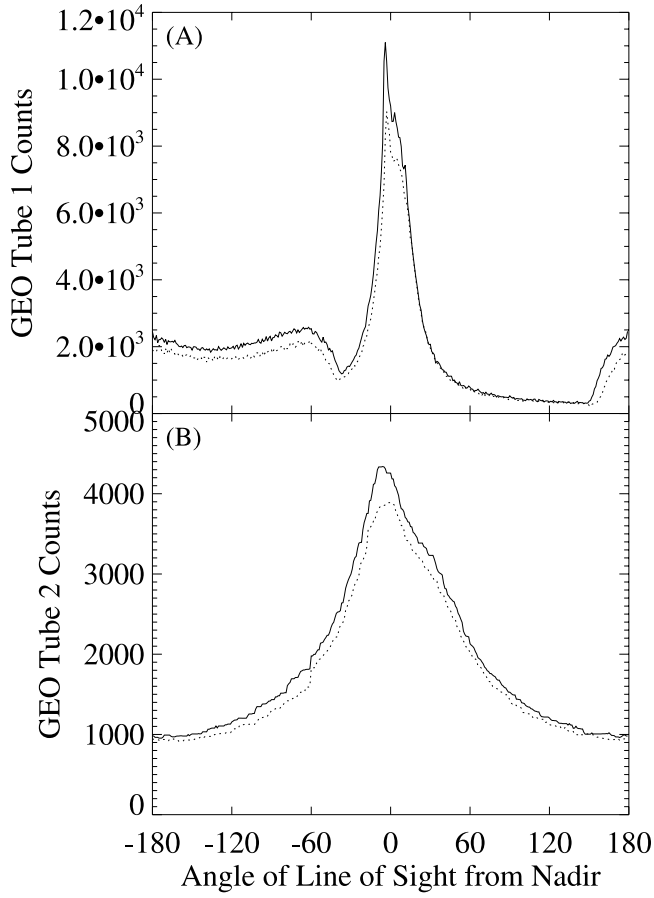

Figure 3. Examples of GEO photometer observations before and during the flare. 3a) GEO Tube 1 observations, where observations at 0° are at the nadir. Solid (dashed) lines show counting rates during (before) the flare. 3b) GEO Tube 2 observations, obtained simultaneously with the measurements shown in Figure 3a.

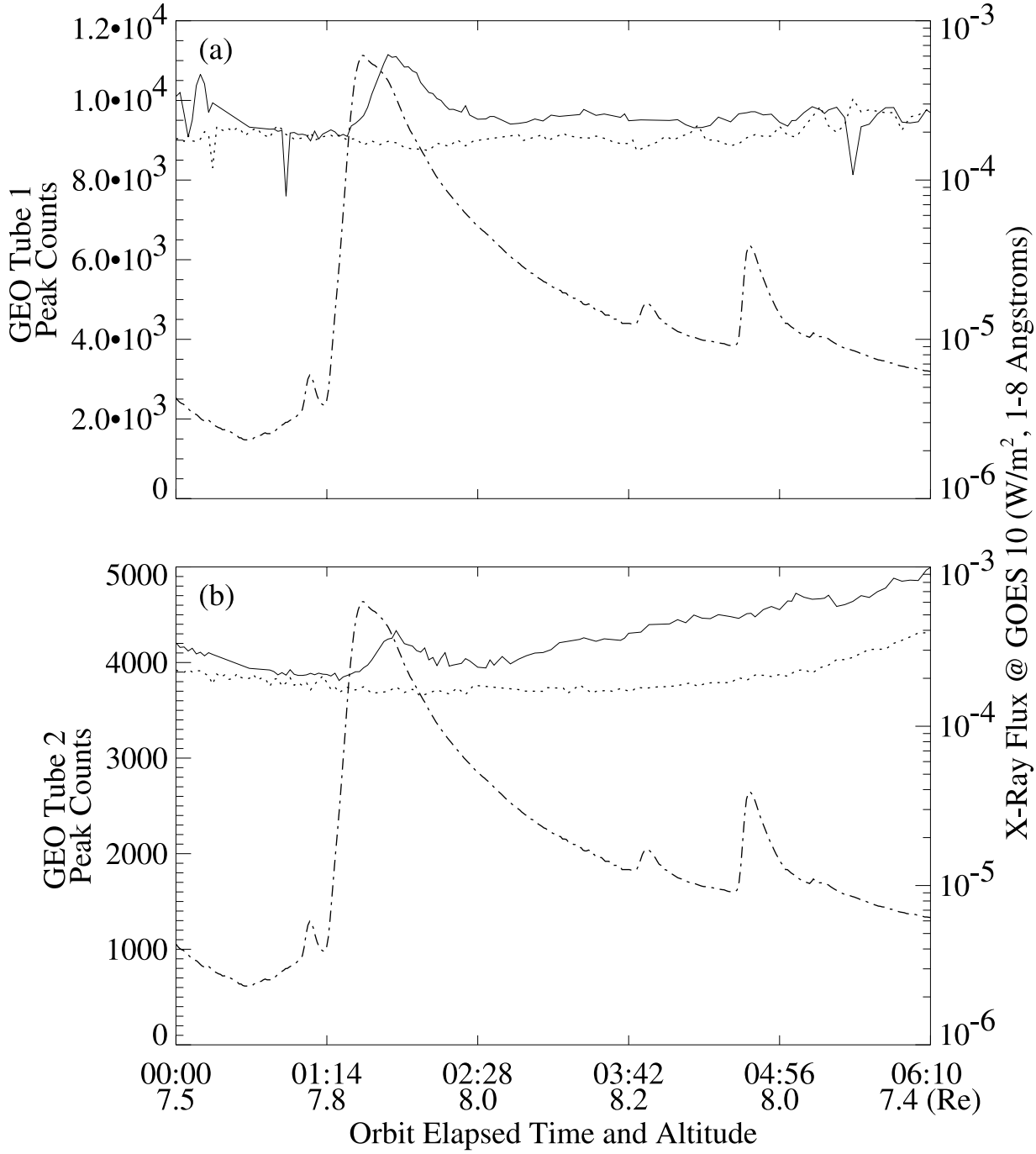

Figure 4. Flare-induced FUV brightness variation measured by two GEO photometers on IMAGE. 4a) The peak response in the FUV GEO tube 1 channel during the flare-time orbit is shown with a solid line, with values obtained during the previous orbit shown with a dotted line. The x-ray flux is shown with a dot-dash line, on a logarithmic scale indicated to the right. Spacecraft altitude in Earth radii are shown below UT on the abcissa. 4b) Same as 4a except now showing the response of GEO tube 2.

Ly-α emissions [*Bishop*, 1999, 2001] with a complete FUV dayglow simulation code described by *Gladstone* [1994], which is usually called the REDISTER code after its partial redistribution resonance scattering component. A comparison of the measured GEO signal to the combined results of these codes is shown in Figure 5. The GEO data are converted to kiloRayleighs (kR) using recent stellar calibrations (N. Østgaard, private communication, 2002) for direct comparison with the models. All the results are reported in terms of effective kR, as the total GEO signal consists of both line-of-sight and scattered light components. This is particularly important for the correct interpretation of the geocoronal Ly-α emissions, where the off-axis contribution to the GEO signal can approach or exceed that from on-axis observations. The dashed line in Figure 5 shows the expected line-of-sight brightness of the geocorona from the Bishop model, which peaks near 20 kR. The dotted line shows the result of adding the predicted off-axis contribution

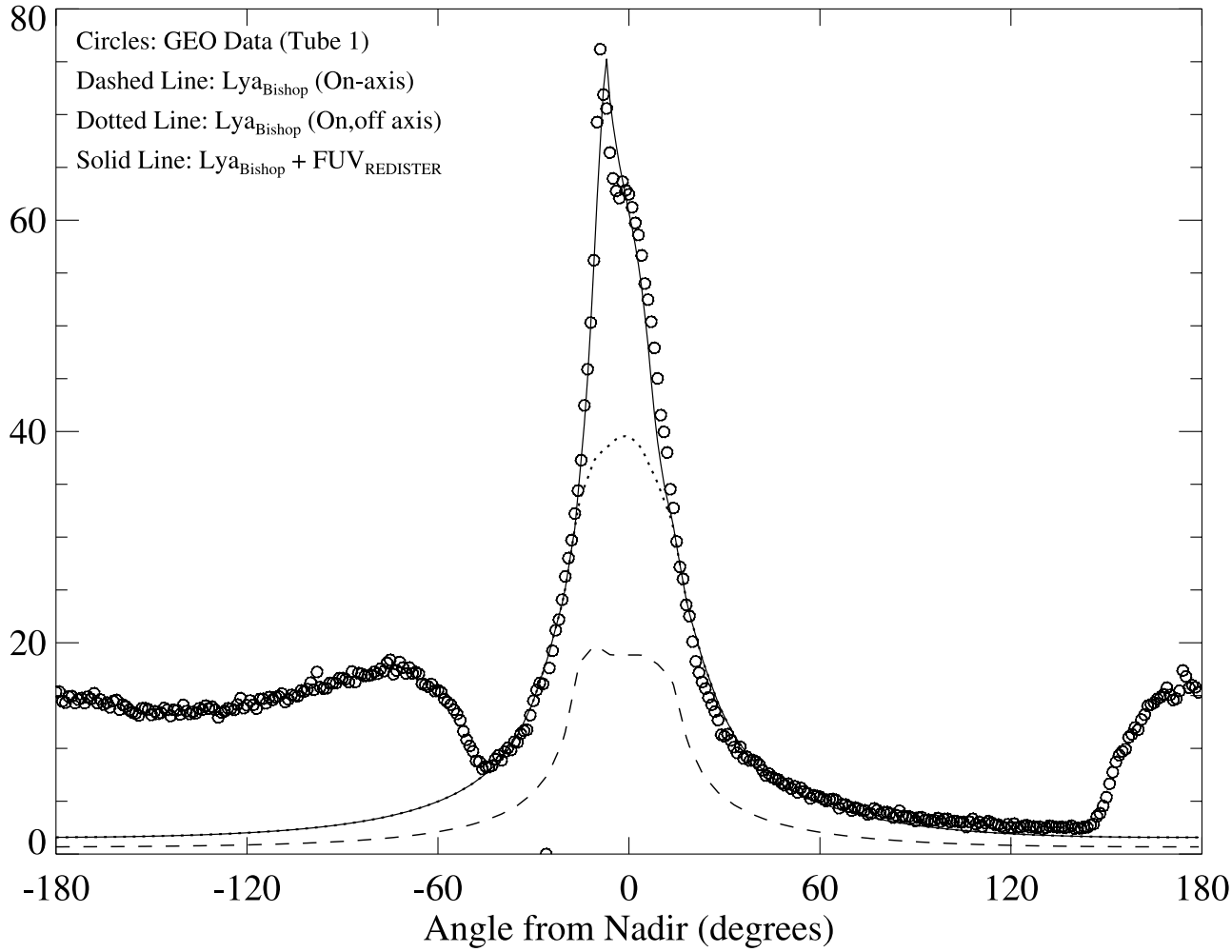

Figure 5. Comparison of GEO Tube-1 response to first-principles modeling results. Bishop's geocoronal H Ly-α model is combined with Gladstone's terrestrial FUV model, and convolved with the GEO instrument response function to simulate the GEO observations over a single spacecraft rotation. The FUV model only has an important effect at angles $<\pm 10^\circ$ from nadir. GEO observations are indicated with open circles. The Bishop model alone is shown with a dashed line, and the with the contribution from scattered geocoronal emissions with a dotted line. The solid line shows the total predicted response of the GEO instrument to the combined Ly-α and FUV emissions.

to that signal. In this case, no scaling or further modification is made to the geocoronal model, and the correspondence between model and data is clearly excellent at angles 15 degrees and more from nadir (Earth itself subtending $\sim 10^\circ$ from the vantage point of 8 Re). The broad area of values exceeding the geocoronal model (below -60° and above 150°) marks a range of measurements contaminated by indirect solar illumination of the photocathode. This contamination does not interfere with the on-Earth observations.

[20] Closer to Earth, FUV emissions of O I and N I contribute to the instrument signal. Modeling of the off-axis GEO response to terrestrial emissions shows them to be a much less significant source (10–15%) of instrument signal than in the case of geocoronal emissions. In that light, only the on-axis contributions are considered. The total FUV emissions (120.0 + 130.4 + 135.6-nm) and the REDISTER Ly-α are scaled separately to match the observed counting rates. The Bishop geocoronal model should account for all terrestrial Ly-α emissions. However, REDISTER Ly-α emissions are included for the following reasons: (1) The predicted O I and N I emissions combined with the Bishop geocoronal model cannot themselves fully account for the GEO signal (considering even off-axis contributions), and (2) The combined profile of the REDISTER O I + N I and Bishop Ly-α emissions exhibits sharp variations at Earth's limb, which are not observed by GEO. To provide the best fit to the GEO data, the combined O I and N I emissions are scaled together to 70% of the initial REDISTER prediction, while the Ly-α emissions are reduced to half the initial prediction. From the combined models, the relative proportion of the combined FUV emissions relative to the total H I background is found to be 0.28 at the peak, and 0.20 at on-Earth points away from the limb. This is important for proceeding toward discovery of the true flare-time variation in the solar 130.4-nm emission.

[21] The next steps in extracting the variation in the O I 130.4-nm solar resonance scattering components involve other parameters from the combined model, namely the

120.0/130.4 and 135.6/130.4 ratios which are determined self consistently in REDISTER. These are approximately 0.08 and 0.04, respectively, at points on the disk, approximately 1–2 degrees from the limb. With all of the parameters here, it is important to avoid observations at the limb, where the 120.0-nm and 135.6-nm emissions vary rapidly with tangent height (e.g., 135.6/130.4 $\simeq$ 0.1 at the limb), as do the relative contributions of resonant and photoelectron O I 130.4-nm emission sources. Furthermore, an estimate of the relative brightness of the resonant and photoelectron sources for O I 130.4 is crucial. For this, one can refer to the case shown in *Meier* [1991, Figures 57, 58] for solar maximum, where it is shown that nadir viewing observations can expect the photoelectron contribution to be approximately twice that from resonant emissions.

[22] This analysis uses GEO measurements two 'pixels' from the limb, where the total observed variation is 17.5%, the relative contributions of 135.6 and 120.0-nm emissions are as stated above and the altitude dependence of resonant/photoelectron 130.4-nm O I contributions no longer can affect the observations. After converting the emission brightnesses to relative instrument counts using the instrument response function described by *Mende et al.* [2000b], the calculation is performed. The final result is that the solar O I 130.4-nm emission is found to vary at flare-time by 16 ± 10%. The uncertainty stems mainly from the statistical uncertainties in the GEO measurements, to which the calculation is quite sensitive, and admits no errors in the modeling. The details of the calculation are reported in Appendix A. This result indicates that the flare-time solar O I variation is significantly higher than the H I Lyα variation.

[23] With the large reported uncertainty, one should look for corroborating evidence that the flare-time solar O I 130.4-nm variation is, in fact, nearly twice the H I variation. One clue may be found in the fact that the contaminating solar light in the GEO tube 1 data, which is manifested as the heightened counting rates at viewing angles well away from Earth in Figure 3a, varies by 31% during the flare, much more than the variation in the geocoronal H I signature. This scattered light consists of solar H I Ly-α emissions as well as O I and C II emissions at 130.4 and 133.5-nm, respectively. The total of these later emissions exceeds the H I brightness [*Curdt et al.*, 2001]. Assuming for now that the C and O emissions are together as bright as the H emission, if the O I line varied by 16% during the flare, the variation required of the C II line to account for the variation in the scattered solar component in the GEO signal would be 100%. Though there is no independent measure of the C II emission during this flare, it likely that the variation is not that large, and that it varies more like a singly ionized emission such as He II at 30.4 nm, which varies by $\sim$54% during this flare (as noted in the next section). Therefore, it is argued that the 16% flare-time variation in solar O I 130.4-nm is very likely a lower limit on the range of possible values, and that the solar 130.4-nm emission varies considerably more than the solar Ly-α emission.

3.3. Comparison of FUV and EUV Observations

[24] Cross-correlation coefficients between the GOES 10 X-Ray flux data and the dayglow brightness observed with the imagers show a good correspondence between these separately determined parameters, with $0.8 < r < 0.9$. However, greatest correlation is obtained if the X-rays are time lagged (shifted to later times) by 3–4 minutes. This, and the 6–8 minutes separation of the FUV and X-Ray peaks, shows that the soft x-rays measured by GOES clearly are not directly related to the major FUV variations. There is another data set that yields a much better comparison: measurements by the SOHO-Solar Extreme-Ultra-Violet Monitor (SEM) experiment. A comparison of data from SOHO-SEM (narrow channel, 26–34 nm) and IMAGE-FUV is shown in Figure 6. All of the FUV channels show a very good correlation with the measured solar EUV, with r = 0.99, 0.98, and 0.97 between the SEM narrow channel and the WIC, SI-13 and SI-12 channels, respectively. The change in the slope of the increasing values around 1020 UT, and the increase in the decay rate after 1040 UT are reflected in both data sets, and is particularly obvious in the WIC channel. Correlations with the SOHO-SEM wide-channel (not shown), which responds to solar emissions between 1 and 50 nm, are slightly less significant, with r = 0.95, 0.94, and 0.90 for WIC, SI-13 and SI-12, respectively.

[25] There are large percent changes in each SEM channel during the flare. The enhancement in the narrow channel is 53.5%, while the wide channel varies by 76.2%. The FUV dayglow variations observed by IMAGE all fall in this range.

[26] Comparisons between the SOHO-SEM data and the GEO photometers are not shown. However, in a comparison of GEO tube 2 (H I @ 121.6 nm only) with SOHO/SEM narrow band observations during the flare, the data are found to correlate well (r = 0.93). This supports the conclusion, inferred earlier from IMAGE observations alone, that the solar EUV and FUV fluxes covary.

3.4. Origin of Variation in SI-12 Channel

[27] The SI-12 data shown in Figure 6 are labeled as emissions of N I @ 120.0-nm. Though this imager is sensitive to Doppler shifted H I emissions, the 76% dayglow variation observed in this channel is indicative of an emission driven by a source which varies more than the solar 121.6-nm emission, which the GEO (tube 2) measurements show varies only by 10%. The imager suppresses the core of this line, but would be sensitive to the long wavelength wing, if that were to be resonantly scattering processes where the optical depth of H I is large. Though this may occur, the character of the dayglow emission in the SI-12 indicates the source constituent has a much smaller scale height than H I. An SI-12 image obtained at 1017 UT, shown in Figure 7, clearly shows that the instrument response originates at locations close to Earth. With increasing tangent heights, counting rates vary from a peak brightness at the limb down to background values over an altitude of one H I scale height (>500 km).

[28] The most probable explanation for the dayglow observations is that the SI-12 instrument is also sensitive to the 120.0-nm triplet emission of N I. Though the imager was designed to suppress this emission, the transmission at 120.0 nm is not insignificant, with 8% transmission at the 120.0-nm minimum vs. 80% at 121.8 nm. Another possibly important N I emission at 124.3 nm is located neither in a peak or a valley of the transmission function (28%). However, this line has been reported to be 10 times as faint as the 120.0-nm line [*Chakrabarti et al.*, 1983]. So, under normal circumstances, $\sim$70% of the SI-12 signal due to N I

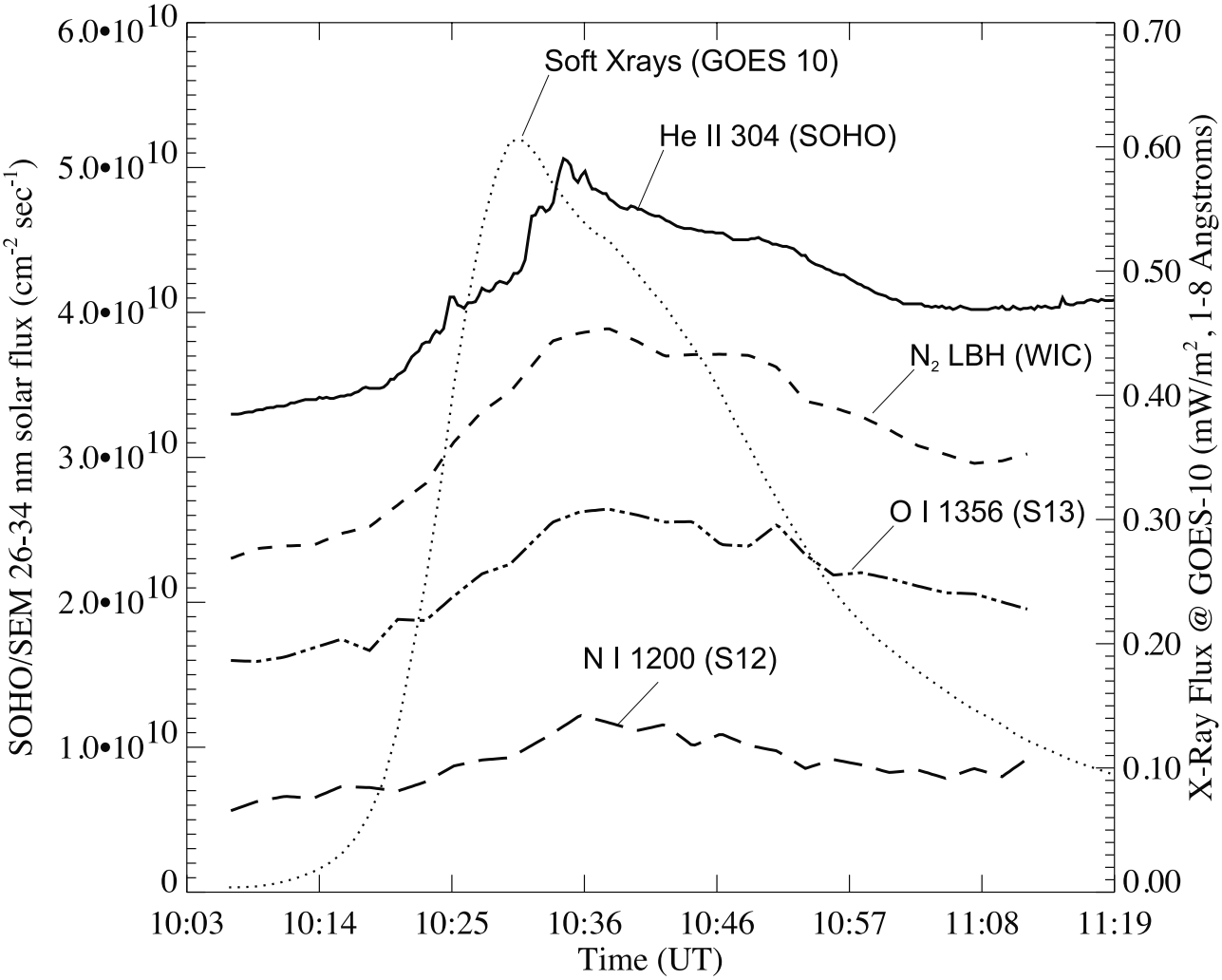

Figure 6. Flare-time variations in IMAGE-FUV and SOHO Charge, Element, and Isotope Analysis System (CELIAS)/SEM responses. The response in the FUV imaging channel is compared to the SOHO/SEM narrow channel, the latter shown with a solid line. The left hand ordinate represents only the SOHO/SEM variation, while the FUV data are independently scaled, though showing the same responses as in Figure 2. The GOES 10 X-Ray data are also shown for reference, now on a linear scale (vs. the format of Figures 1 and 2).

emissions will be from the 120.0-nm line, with the remainder attributable to 124.3-nm emissions.

[29] These dayglow emissions are driven primarily by photodissociative excitation of N_2 in the thermosphere, which leads to two N I atoms, or a combination of N I and N II. The total cross sections for these two processes are shown as a function of photon wavelength in Figure 8 (top) [*Kronebusch and Berkowitz*, 1976]. The wavelength ranges where photons have enough energy to produce N I in the excited N I(^{4}P) state are indicated with double-ended arrows below the N_2 cross section data. These cross sections can be convolved with a model solar EUV spectrum (here the Solar2000 model spectrum is used [*Tobiska et al.*, 2000]) to calculate the relative importance of solar emissions in producing N I(^{4}P). This is done assuming that the processes short and longward of 50.0 nm both result in the excited N I(^{4}P) state which can produce emissions at 120.0 nm. Such a calculation shows that solar EUV emissions shortward of ~50.0 nm are of primary importance in producing N I 120.0-nm. The relative importance of the two wavelength regimes is shown in Figure 8 (bottom), where we use the Solar2000 spectrum for 21 January 1991, when the solar 10.7-cm radio flux is similarly high as the time prior to the Bastille Day flare.

[30] The greatest single contributor to N I production is from the He II line at 30.4 nm (~20%), but a greater overall contribution comes from emissions shortward of 30 nm (~55%). From the SEM wide-channel observations, it is clear that the variation in these shorter wavelength emissions is larger than the variation in the He II 30.4-nm line (which varies only by 54%). Indeed, the total variation in the solar spectrum between 1 and 50 nm is 76%, nearly identical to the observed N I variation.

4. Conclusion

[31] This work shows that during the Bastille Day flare, the terrestrial FUV emissions measured by IMAGE nearly

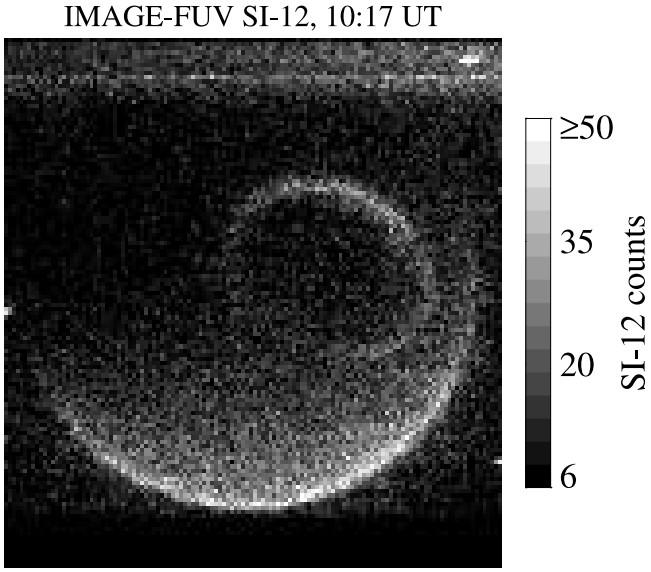

Figure 7. SI-12 image before peak solar EUV output. N I 120.0-nm dayglow emissions and Earth's limb are clearly visible in this original image. The Sun direction is to the lower right.

covary with the EUV emissions of the Sun, and that the x-rays in the $\lambda = .1-.8$ nm range precede the peak in terrestrial EUV and FUV emissions by 6–8 minutes. It is generally understood that terrestrial photoelectrons are created by both soft x-rays and EUV. If x-rays do contribute to the dayglow enhancements observed here, it is those longward of 1.3 nm, considering a linear extrapolation of the one-minute difference between time of the peak response in the two GOES channels centered at 0.225 and 0.45 nm, respectively. The latter (longer) of these two channels is shown in Figures 1, 2, 4, and 6. The solar EUV emissions are shown to be the primary source of the variation in all the airglow channels.

[32] Using the combined observations of SI-13 and GEO tubes 1 and 2, the flare-time variation in the solar O I 130.4-nm line is shown to be 16 ± 10%, greater than that of the H I 121.6-nm line (10.2%). This is determined, in part, by requiring that the photoelectron-produced component of the terrestrial 130.4-nm emission be greater than the resonantly scattered component, and through modeling of the contributions to the GEO signal. Evidence provided by analysis of the scattered solar light present in the data suggests that the variation in the solar O I line is in the high end of the reported range of uncertainty. This is somewhat unexpected, as the solar O I emission is known to be closely related to solar H I Lyman-β emissions at 102.6 nm (the O I emission is, in fact, pumped by the H I emission [*Gladstone*, 1992]). This H I emission should vary similarly to the Ly-α emission, which in this case varies only by 10%. Further study and modeling of the GEO signal during flares would help clarify this apparent discrepancy.

[33] That the terrestrial LBH and 135.6-nm emissions vary by 65% and 68%, respectively, while the 120.0-nm line varies by 76%, shows the inherent difference between emissions resulting from photoelectron impact and those from photodissociation. The primary source for photoelectrons of energies sufficient to excite FUV emissions (>∼10 eV) is photoionization of N_2, O I and O_2 by solar EUV shortward of 50 nm. The combined cross section for the $N_2 + h\nu \rightarrow N_2^+ + e$ and $N_2 + h\nu \rightarrow N + N^+ + e$ reactions is shown with a dot-dashed line in Figure 8 (top) [*Kronebusch and Berkowitz*, 1976]. It is immediately clear that the total N_2 photoionization cross section is larger than the dissociative ionization cross section (shown with a solid line and described in section 3.4). The total ionization cross section does not peak around 22 nm and drop at longer wavelengths like the N_2 photodissociation cross section. Rather, it increases toward higher wavelengths. The total photoionization cross sections for O I and O_2 (not shown), have a similar character [*Brion et al.*, 1979; *Richards and Torr*, 1984].

[34] The result is that photoelectron production is dominated by emissions longward of 30.0 nm, including the 30.4-nm emission measured by SEM, whereas production of excited N I atoms through photodissociation is predominately by emissions shortward of 30.0 nm. Emissions $\lambda <$ 30.0 nm only contribute 18.6% to the production of photoelectrons from N_2 with energies >10 eV required for subsequent excitation of FUV emissions (shown in Figure 8), while they are responsible for more than half of the N I

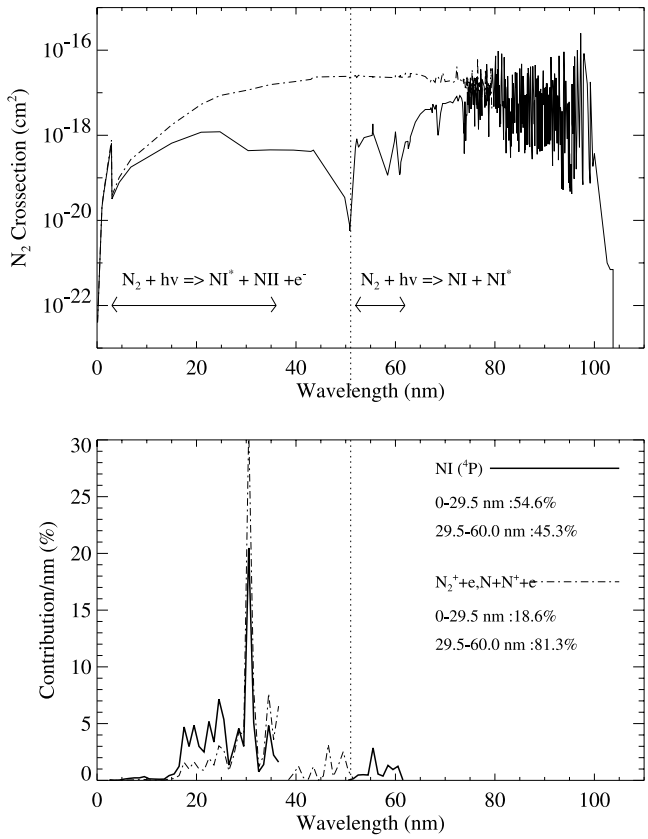

Figure 8. Cross sections and relative contributions to production of N I. top) Photodissociation cross sections (solid line) for N_2 for the production of 2 neutral N atoms ($\lambda >$ 51.0 nm) or an ion and a neutral ($\lambda <$ 51.0 nm). The total photoionization cross-section for N_2 is also shown (dot-dashed line). Arrows indicate ranges where the products may be excited to a state to produce 120.0-nm emissions. bottom) Relative contributions of solar EUV emissions to production of excited N I atoms.

120.0-nm emission. As noted earlier in this report, the signal in the SEM narrow channel varies by 53.5%, but in the wide channel by 76.2%. The latter is sensitive to solar lines down to 1 nm, where the narrow channel is sensitive mainly to He II 30.4-nm emissions. It is clear, therefore, that the dayglow emissions observed in the SI-12 channel are driven by shorter wavelength emissions, which are more important in the production of N I and terrestrial 120.0-nm emissions, which vary more significantly during the flare.

[35] Recently, the WIC instrument's sensitivity to UV emissions in the 200–300-nm range has been the subject of some discussion [*Gladstone*, 2000]. This work provides evidence against a substantial contribution of long wavelengths to the total WIC response, as the variation in WIC with the flare is very close to that which one expects for an instrument sensitive in the 140–190-nm range [*Opal*, 1973]. This channel also shows a flare-time variation very similar to that of the SI-13 channel, which also measures emissions produced primarily by photoelectron impact. Furthermore the variation in the WIC channel is comparable to that observed in images obtained by the POLAR satellite. POLAR UVI images using the LBH-long filter show a flare-time increase in dayglow emissions of approximately 70% [G. Parks, Private Communications, 2001]. Any discussion of the contribution of long-wavelength emissions to the WIC signal must also account for the large flare-time variation seen here. If it is indeed found that the WIC instrument has a significant sensitivity in the MUV (180.0–220.0 nm), then this could suggest that the Bastille Day flare had a strong MUV component. This would be a surprising finding, since flare-time variations in continuum solar MUV emissions are normally expected to be insignificant in comparison to EUV and FUV variations.

[36] Several large flares have occurred since the launch of IMAGE, and the spacecraft was often ideally located for studies of their terrestrial effects. Further studies and modeling of flare-induced variations in terrestrial FUV emissions can reveal new understanding of the Sun-Earth connection during these powerful events. Examination of the SI and WIC images shows little contamination from high-energy protons streaming from the flare region, relative to various other space-borne instruments, including both imagers and particle detectors. IMAGE-FUV is therefore well suited for studies in space and solar physics as an all-space-weather instrument.

Appendix A: Method of Deriving Flare-Time Solar O I 130.4-nm Variation From Combination of FUV Observations and Modeling Results

[37] The total response of the GEO instrument prior to, and at the peak of, the flare is given as:

$$GEO_I = Ly_I + FUV_I \tag{A1}$$

and

$$GEO_F = Ly_I * R_{Lya} + FUV_I * R_{FUV}, \tag{A2}$$

where Ly_I and FUV_I are the initial contributions of the H I and all remaining emissions to the GEO signal, respectively. The ratios $R_{Lya,FUV}$ are the ratios of the flare-time contribution to the preflare contribution. In the case of R_{Lya}, this is known from the GEO tube 2 results to be 1.102.

[38] Now express all terms as functions of Ly_I by letting

$$X = FUV_I/Ly_I \qquad \text{and} \qquad Y = GEO_F/GEO_I.$$

Using Y to equate A1 and A2, then solving for R_{FUV} yields

$$R_{FUV} = \frac{\left[Y*(X+1) - R_{Lya}\right]}{X}. \tag{A3}$$

With X determined from the modeling results in section 3.2, and Y from the GEO tube 1 observations (on-Earth), the change in the FUV emissions can be solved for.

[39] Now explicitly, that change is equal to the following:

$$R_{FUV} = \frac{1200_F + 1356_F + 1304_F}{1200_I + 1356_I + 1304_I} \tag{A4}$$

To express all terms on the right side as functions of 1304_I, let

$$a = 1200_I/1304_I, \qquad b = 1356_I/1304_I,$$

$$c = 1200_F/1200_I, \qquad d = 1356_F/1356_I$$

$$\text{and} \quad \mathrm{Z} = 1304_\mathrm{F}/1304_\mathrm{I}$$

Substituting and solving for Z yields

$$Z = R_{FUV}*(a+b+1) - ac - bd \tag{A5}$$

Z represents the total change in 130.4-nm emissions. This can be solved for, as a and b are determined in the modeling results in section 3.2, c and d are known from the variations in the SI-12 and -13 channels, respectively. R_{FUV} was determined in A3.

[40] Acknowledging now that the 130.4-nm emission has a photoelectron (PE) and resonant (Res) component, express Z in terms of the initial and final magnitude of those components.

$$Z = \frac{1304_F}{1304_I}$$

$$= \frac{PE_F + Res_F}{PE_I + Res_I} \tag{A6}$$

$$= \frac{\gamma PE_I + \alpha Res_I}{PE_I + Res_I} \tag{A7}$$

Here $\alpha = Res_F/Res_I$ and $\gamma = PE_F/PE_I$ have been substituted. Now using $\beta = PE_I/R_I$, express each term as a function of Res_I and solve for α. This yields

$$\alpha = Z(\beta + 1) - \gamma\beta \tag{A8}$$

which is the ratio of flare-time to preflare 130.4-nm resonant emissions on Earth. This is directly related to the change in the solar 130.4-nm line during the flare. This can

now be calculated using values of β from simulations [*Meier*, 1991], and values of γ from the SI-13 observations.

[41] **Acknowledgments.** The IMAGE-FUV investigation was supported by NASA through Southwest Research Institute subcontract number 83820 at the University of California, Berkeley, contract NAS5-96020. We are grateful to D. Judge and the SOHO team for providing the CELIAS/SEM data. SOLAR2000 Research Grade v1.15 historical irradiances are provided courtesy of W. Kent Tobiska and SpaceWx.com. These historical irradiances have been developed with funding from the NASA UARS, TIMED, and SOHO missions. Thanks also go to Dr. R. Link for numerous helpful discussions.

[42] Shadia Rifai Habbal thanks both referees for their assistance in evaluating this paper.

References

Bailey, S. M., Response of the upper atmosphere to variations in the solar x-ray irradiance, Ph.D. thesis, Univ. of Colo., Boulder, 1995.

Bishop, J., Transport of resonant atomic hydrogen emission in the thermosphere and geocorona: Model description and applications, *J. Quant. Spectrosc. Radiat. Transfer*, *61*, 473–491, 1999.

Bishop, J., Thermospheric atomic hydrogen densities and fluxes from dayside Lyman α measurements, *J. Atmos. Sol. Terr. Phys.*, *63*, 331–340, 2001.

Brion, C. E., K. H. Tan, M. J. V. D. Wiel, and P. E. V. D. Leeuw, Dipole oscillator strengths for the photoabsorption, photoionization and fragmentation of molecular oxygen, *J. Electron Spectros. Relat. Phenom.*, *17*, 101–119, 1979.

Chakrabarti, S., F. Paresce, S. Bowyer, R. Kimble, and S. Kumar, The extreme ultraviolet day airglow, *J. Geophys. Res.*, *88*, 4898–4904, 1983.

Curdt, W., P. Brekke, U. Feldman, K. Wilhelm, B. N. Dwivedi, U. Schuhle, and P. Lemaire, The SUMER spectral atlas of solar disk features, *Astron. Astrophys.*, *375*, 591–613, 2001.

Donnelly, R. F., Empirical models of solar flare X-ray and EUV emission for use in studying their E and F region effects., *J. Geophys. Res.*, *81*, 4745–4753, 1976.

Gladstone, G. R., Solar O I 1304-Å triplet line profiles, *J. Geophys. Res.*, *97*, 19,519–19,525, 1992.

Gladstone, G. R., Simulations of DE 1 UV airglow images, *J. Geophys. Res.*, *99*, 11,441–11,448, 1994.

Gladstone, G. R., Stellar calibration of the WIC and SI imagers and the GEO photometers on IMAGE/FUV, *Eos. Trans. AGU*, *81*(48), F1034, Fall Meet. Supp., 2000.

Hall, L. A., Solar flares in the extreme ultraviolet, *Sol. Phys.*, *21*, 167–175, 1971.

Hall, L. A., and H. E. Hinteregger, Solar EUV enhancements associated with flares, in *Solar Flares and Space Research*, edited by C. D. Jager and Z. Švestka, pp. 81–86, North-Holland, New York, 1969.

Horan, D. M., and R. W. Kreplin, Measurements of solar EUV and soft x-ray emission during sudden frequency deviations, *J. Geophys. Res.*, *85*, 4257–4269, 1980.

Kronebusch, P. L., and J. Berkowitz, Photodissociative ionization in the 21–41 ev region: O_2, N_2, CO, NO, CO_2, NH_3 and CH_4, *Int. J. Mass Spectrom. Ion Phys.*, *22*, 123–136, 1976.

Liu, J. Y., C. S. Chiu, and C. H. Lin, The solar flare radiation responsible for sudden frequency deviation and geomagnetic fluctuation, *J. Geophys. Res.*, *101*, 10,855–10,862, 1996.

Meier, R. R., Ultraviolet spectroscopy and remote sensing of the upper atmosphere, *Space Sci. Rev.*, *58*, 1–185, 1991.

Mende, S. B., et al., Far ultraviolet imaging from the IMAGE spacecraft. 2, Wideband FUV imaging, *Space Sci. Rev.*, *91*, 271–285, 2000a.

Mende, S. B., et al., Far ultraviolet imaging from the IMAGE spacecraft. 3. Spectral imaging of Lyman-α and OI 135.6 nm, *Space Sci. Rev.*, *91*, 287–318, 2000b.

Opal, C. B., Enhancements of the photoelectron-excited dayglow during solar flares, *Adv. Space Res.*, *13*, 797–802, 1973.

Parks, G. K., and J. R. Winckler, The relation of energetic solar x-rays ($h\nu >$ 60 keV) and high frequency microwaves deduced from the periodic bursts of August 8, 1968 flare, *Sol. Phys.*, *16*, 186–197, 1971.

Prinz, D. K., and R. R. Meier, Ogo-4 observations of the Lyman-Birge-Hopfield emission in the day airglow, *J. Geophys. Res.*, *76*, 6146–6158, 1971.

Reid, G. C., and C. Collins, Observations of abnormal VHF radio wave absorption at medium and high altitudes, *J. Atmos. Terr. Phys.*, *14*, 63–81, 1959.

Richards, P. G., and D. G. Torr, An investigation of the consistency of the ionospheric measurements of the photoelectron flux and solar EUV flux, *J. Geophys. Res.*, *89*, 5625–5635, 1984.

Tobiska, W. K., T. Woods, F. Eparvier, R. Viereck, L. Floyd, D. Bouwer, G. Rottman, and O. R. White, The SOLAR2000 empirical solar irradiance model and forecast tool, *J. Atmos. Sol. Terr. Phys.*, *62*, 1233–1250, 2000.

Walker, A. B. C., Jr., and H. G. Rugge, Enhancement of the solar x-ray spectrum below 25Å during solar flares, in *Solar Flares and Space Research*, edited by C. de Jager and Z. Švestka, pp. 102–112, North-Holland, New York, 1969.

H. U. Frey, T. J. Immel, S. B. Mende, and N. Østgaard, Space Sciences Laboratory, University of California, Berkeley, CA 94720, USA. (immel@ssl.berkeley.edu)

G. R. Gladstone, Southwest Research Institute, 6220 Culebra Road, San Antonio, TX 78238-5166, USA.